
Events as Triggers for Behavioral Diversity in Multi-Agent Reinforcement Learning

Hannes Büchi Manon Flageat* Eduardo Sebastián* Amanda Prorok
Department of Computer Science and Technology, University of Cambridge, UK
{hmb71, mf873, es2121, asp45}@cam.ac.uk

Abstract

Effective multi-agent cooperation requires agents to adopt diverse behaviors as task conditions evolve—and to do so at the right moment. Yet, current Multi-Agent Reinforcement Learning (MARL) frameworks that facilitate this diversity are still limited by the fact that they bind fixed behaviors to fixed agent identities. Consequently, they are ill-equipped for tasks where agents need to take on different roles at very specific moments in time. We argue that, to define these behavioral transitions, the missing ingredient is **events**. Events are changes in the state of the system that induce qualitative changes in the task. Based on this view, we introduce a framework that decouples agent identity from behavior, capturing a continuous manifold from which agents instantiate their behaviors in response to events. This framework is based on two elements. First, to build an expressive behavior manifold, we introduce Neural Manifold Diversity (NMD), a formal distance metric that remains well-defined when behaviors are transient and agent-agnostic. Second, we use an event-based hypernetwork that generates Low-Rank Adaptation (LoRA) modules over a shared team policy, enabling on-the-fly agent-policy reconfiguration in response to events. We prove that this construction ensures that diversity does not interfere with reward maximization by design. Empirical results demonstrate that our framework outperforms established baselines across benchmarks while exhibiting zero-shot generalization, and being the only method that solves tasks requiring sequential behavior reassignment.

1 Introduction

Effective cooperation in multi-agent systems hinges less on agent identity than on agent behavior at any given moment. As tasks unfold, optimal team performance demands that agents adapt their behaviors dynamically, not uniformly across the team nor on a synchronized schedule, but at the right moment and under the right circumstances. When a quadrotor in a search team loses power, the remaining agents expand their coverage to compensate; or a defender in football pushes forward only once possession changes to the other team. These transitions are not arbitrary but triggered by events. Events are changes in the system’s state—e.g., team composition and environment configuration—that induce qualitative changes in the task and demand a behavioral response.

Behavioral diversity, or behavioral heterogeneity, is a key driver of performance in cooperative Multi-Agent Reinforcement Learning (MARL) [Li et al., 2021], and recent approaches have proposed various ways to introduce it within agent teams [Bettini et al., 2023]. Yet few existing approaches capture dynamic behavior adaptation. Most either assign behaviors statically, fixing each agent’s role for the entire episode, or periodically, switching every few time steps regardless of context. We argue that this gap reflects a deeper conceptual issue. Whether diversity is enforced via unique per-agent heterogeneous components in the policy [Bettini et al., 2024a], agent-specific weights generated by

*Equal contribution.

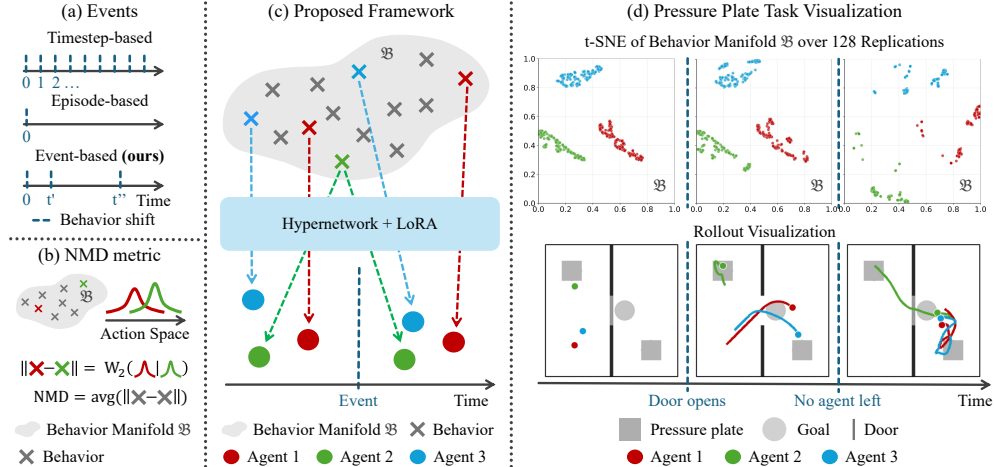


Figure 1: **Proposed Framework.** (a) Rather than shifting behaviors on a fixed timestep or episode schedule, our framework triggers behavioral transitions in response to task events. We realize this through two components: (b) NMD, a diversity metric defined directly on the behavior manifold and independent of which agent executes which behavior; and (c) an event-driven hypernetwork that generates LoRA [Hu et al., 2022] modules over a shared policy to allocate behaviors from the manifold. (d) We visualize the behavior manifold via a two-dimensional t-SNE projection across 128 replications of the Pressure Plate environment, alongside agent trajectories for one rollout.

a hypernetwork [Tessera et al., 2025], or partitioned action spaces [Wang et al., 2020b], existing approaches share the same implicit assumption: behaviors are tied to specific agents.

We challenge this assumption. We view behaviors as a property of the task—a continuous manifold the team draws from—whose traversal is dictated by events rather than by agent identity. Decoupling behavior and identity reframes the central question of diversity in MARL: rather than asking how to differentiate agents, we ask how to populate, structure and navigate the behavior manifold.

This brings three requirements. First, to ensure the manifold is genuinely diverse, we need a metric defined directly on behaviors rather than on agents. We introduce Neural Manifold Diversity (NMD), which measures diversity in the behavior manifold directly, independent of the agents currently executing those behaviors. Second, we need an architecture that can both learn such a manifold and adapt agents as events unfold. We achieve this through an event-based hypernetwork that generates Low-Rank Adaptation (LoRA) [Hu et al., 2022] modules over a shared team policy, a computationally efficient alternative to full policy regeneration. Third, we need an optimization procedure that jointly maximizes team reward while preserving manifold diversity. We adopt a diversity-constrained objective [Bettini et al., 2024a], and prove that this construction does not interfere with reward maximization by design. Fig. 1 illustrates our framework. In summary, our contributions are:

- We introduce an event-centric paradigm in which agents draw their behaviors dynamically from a continuous manifold, adapting in response to events.
- We propose a behavior-centric metric, NMD, that models diversity directly within this manifold, independent of which agent executes which behavior.
- We realize the framework through an event-driven hypernetwork generating LoRA modules. We prove that this architecture aligns task-objective gradients with NMD constraints through diversity control, guaranteeing joint reward maximization and diversity preservation.

2 Related Work

A variety of MARL approaches investigate the allocation of diverse behaviors (also frequently referred to as “roles”) within a team. We review the most closely related work along three axes, and refer the reader to Appendix A for an extended discussion.

Temporal Behavioral Assignment. A core question for behavior allocation is the assignment timeline. Existing approaches fall into two categories: methods that fix one behavior per agent for the entire episode [Tessera et al., 2025, Bettini et al., 2024a, Jiang and Lu, 2021, Li et al., 2021], and methods that adapt behaviors on a fixed temporal schedule regardless of task conditions [Fu et al., 2025, Qi et al., 2026, Mahajan et al., 2019, Wang et al., 2020a, Goel et al., 2025]. We advocate for a third category: event-based allocation, in which behavioral shifts are triggered by state changes rather than fixed schedules or episode boundaries.

Representations of Behaviors. Behavioral specialization is fundamentally constrained by the underlying behavior representation. Existing approaches include learning explicit per-behavior policies or policy deviations [Jiang and Lu, 2021, Li et al., 2021, Bettini et al., 2024a, Christianos et al., 2021, Kim and Sung, 2023, Li et al., 2024], conditioning a shared policy on agent identity or capabilities [Tessera et al., 2025, Fu et al., 2025, Deka and Sycara, 2021], and learning a latent behavior space to condition a shared policy or hypernetwork [Mahajan et al., 2019, Wang et al., 2020a]. Our framework builds on similar representations but conditions behavior generation on task events, enabling dynamic allocation that prior approaches cannot support.

Quantifying and Enforcing Behavioral Diversity. Existing methods to encourage diversity fall into two categories: auxiliary rewards or losses [Wang et al., 2020a, Li et al., 2021, Mahajan et al., 2019, Jiang and Lu, 2021], which provide no formal guarantee on final team diversity; and hard constraints [Bettini et al., 2024a, Tan et al., 2023], which provide stronger guarantees but require a target diversity value a priori. Diversity is commonly quantified via information-theoretic objectives [Wang et al., 2020a, Li et al., 2021, Mahajan et al., 2019, Jiang and Lu, 2021] or explicit metrics such as System Neural Diversity (SND) [Bettini et al., 2025]. We propose NMD, a new metric inspired by SND that remains well-defined under dynamic behavior allocation, and use it within a constrained optimization framework to enforce target diversity levels.

3 Background

Cooperative Multi-Agent Reinforcement Learning. We model cooperative multi-agent tasks as Partially Observable Markov Games (POMGs) [Shapley, 1953], defined by the tuple $\mathcal{M} = \langle \mathcal{N}, \mathcal{S}, \mathcal{A}, \mathcal{O}, \mathcal{P}, \Omega, \mathcal{R}, \gamma, \mathcal{B} \rangle$. Here, \mathcal{N} is the set of agents, \mathcal{S} the state space, \mathcal{A} and \mathcal{O} the joint action and observation space, \mathcal{P} the transition dynamics, Ω the observation function, \mathcal{R} the shared reward function, and $\gamma \in [0, 1)$ is the discount factor. We additionally let \mathcal{B} denote the **behavior manifold** of \mathcal{M} , i.e., the space of admissible policies $\pi : \mathcal{O} \rightarrow \mathcal{P}(\mathcal{A})$ that the task supports. In this sense, \mathcal{B} is a property of the task—its structure and coverage are determined by what strategies \mathcal{M} admits—and is not given a priori; how to represent and learn it is the central concern of Section 4. Each agent $i \in \mathcal{N}$ executes a policy $\pi_i(a_{i,t} | o_{i,t}) \in \mathcal{B}$, and the team objective is to find a joint policy π^* maximizing the expected discounted return $R = \mathbb{E}[\sum_{t=0}^{\infty} \gamma^t \sum_{i \in \mathcal{N}} r_{i,t}]$. Note that a consequence of this formulation is that a behavior is equivalent to a policy, so we use these terms as interchangeable. We also remark that the observation vector $o_i \in \mathcal{O}$ includes a physical capability descriptor when relevant for the task, in contrast to existing approaches where physical capabilities are defined as independent quantities. We do this to emphasize that our focus is on behavioral diversity, in which agents display different action distributions given identical inputs, rather than physical diversity.

Events as Triggers of Behavioral Change. Standard POMGs treat all transitions as instances of the same dynamics \mathcal{P} , leaving no formal distinction between qualitative changes in task progress. To capture such moments, we augment the POMG with a discrete **event space** Ξ and an **event-detection function** $\mathcal{E} : \mathcal{S} \rightarrow \Xi \cup \{\emptyset\}$ that maps the current state of the system to either a triggered event $\xi_t \in \Xi$ or the null symbol \emptyset , i.e., no event happened. Roughly speaking, an event is a change in the system state—including team composition and environment configuration—that induces a qualitative shift in the optimal joint behavior. Events may originate from distinct sources. In our empirical study, we consider the following cases: changes in an agent’s own observations (e.g., a LiDAR detecting a target); changes in the team configuration (e.g., an agent being added); or environmental signals (e.g., a door opening). When an event triggers, it induces a non-stationary transition $(s_t, \mathcal{N}_t, \mathbf{b}_t) \xrightarrow{\xi_t} (s_{t+1}, \mathcal{N}_{t+1}, \mathbf{b}_{t+1})$ that displaces the system onto a new optimal trajectory manifold, where $\mathbf{b}_t = (\pi_{1,t}, \dots, \pi_{|\mathcal{N}_t|,t}) \in \mathcal{B}^{|\mathcal{N}_t|}$. The challenge for the team is to respond to ξ_t by adapting the behaviors of its members. We refer to the resulting setting as an **Event-Augmented POMG**, defined, with an abuse of notation, as $\mathcal{M} = \langle \mathcal{N}, \mathcal{S}, \mathcal{A}, \mathcal{O}, \mathcal{P}, \Omega, \mathcal{R}, \gamma, \mathcal{B}, \Xi, \mathcal{E} \rangle$.

Problem Formulation. Given \mathcal{M} , our goal is to learn a mechanism that decouples agent identity from executed behavior. Concretely, we seek to learn (1) the continuous behavior manifold \mathcal{B} that captures the space of behaviors admitted in a task, and (2) an event-conditioned mechanism $f : \mathcal{O} \times \Xi \rightarrow \mathcal{B}$ that maps each agent’s observation and most recent event to a behavior $\pi_{i,t} \in \mathcal{B}$. Beyond maximizing cumulative reward, if behaviors are truly properties of the task only, the mechanism should generalize zero-shot as any of the following vary: (1) number of agents, (2) physical capabilities, and (3) event sequences, including disruptions unseen during training (e.g., abrupt teammate removal).

4 A Framework for Event-Driven Behavioral Adaptation

To describe our framework, we proceed in three steps. First, we introduce NMD (Neural Manifold Diversity), the metric that characterizes the behavior manifold \mathcal{B} (Section 4.1). Second, we present its architectural realization: an event-driven hypernetwork that generates LoRA modules over a shared policy backbone that allows us to learn \mathcal{B} and allocate policies to agents according to it (Section 4.2). Third, we describe how diversity is maintained and controlled on \mathcal{B} and we state the theoretical guarantees that follow from this construction, deferring proofs to Appendix B (Section 4.3).

4.1 Modeling the Behavior Manifold: Neural Manifold Diversity

The behavior manifold \mathcal{B} is the central object our framework manipulates: agents draw from it, events trigger movement within it, and its geometry determines what coordination strategies the team has available. To make this manifold a tractable object—one we can measure and control—we begin by quantifying the diversity of policies drawn from it.

Definition 1. Let \mathcal{B} denote the continuous behavior manifold induced by the task \mathcal{M} and let $p(\pi)$ denote a probability density over \mathcal{B} . The Neural Manifold Diversity is the expected pairwise divergence between behaviors sampled from \mathcal{B} , evaluated over the observation distribution $p(o)$:

$$\text{NMD}(\mathcal{B}, \mathcal{O}) = \int_{\mathcal{B}} \int_{\mathcal{B}} \int_{\mathcal{O}} W_2(\pi_m(o), \pi_n(o)) p(o) do p(\pi_m) d\pi_m p(\pi_n) d\pi_n, \quad (1)$$

where W_2 is the 2-Wasserstein distance between action distributions.

A property that justifies treating NMD as a principled diversity measure rather than an arbitrary statistic is that the pairwise term in Eq. (1) defines a proper distance on \mathcal{B} .

Proposition 2. Let $d : \mathcal{B} \times \mathcal{B} \rightarrow \mathbb{R}_{\geq 0}$ be $d(\pi_m, \pi_n) := \mathbb{E}_{o \sim p(o)} [W_2(\pi_m(o), \pi_n(o))]$. Then d is a pseudometric on \mathcal{B} , and a metric whenever policies are distinguishable on the support of $p(o)$.

The proposition guarantees that d satisfies non-negativity, symmetry, identity of indiscernibles (up to $p(o)$ not belonging to a null set), and the triangle inequality. As a consequence, $\text{NMD}(\mathcal{B}, \mathcal{O})$ admits a clear interpretation: it is the expected d -distance between two behaviors drawn independently from \mathcal{B} . The problem with Eq. (1) is that it is intractable because \mathcal{B} and \mathcal{O} are continuous and high-dimensional. In practice, we instantiate a finite collection of policies $\{\pi_m\}_{m=1}^B$ of behaviors and we observe a finite set of episodic observations $\mathcal{O}_{\text{ep}} \subset \mathcal{O}$, substituting the integrals with empirical averages to yield to an estimator:

$$\widehat{\text{NMD}}(\{\pi_m\}_{m=1}^B) = \frac{2}{B(B-1)|\mathcal{O}_{\text{ep}}|} \sum_{m=1}^B \sum_{n=m+1}^B \sum_{o \in \mathcal{O}_{\text{ep}}} W_2(\pi_m(o), \pi_n(o)). \quad (2)$$

This is an unbiased statistic for $\text{NMD}(\mathcal{B}, \mathcal{O})$ whenever the sampled behaviors are i.i.d. In our implementation, $\{\pi_m\}_{m=1}^B$ is the set of behaviors in a parallel batch of environments and \mathcal{O}_{ep} is the set of observations encountered along the rollout.

Structurally, Eqs. (1) and (2) resemble that of SND [Bettini et al., 2025] because it also poses diversity as a distance in action distribution. However, the most important aspect of NMD is what is absent from it: agent indices. Existing metrics, including SND, compute pairwise distances between policies indexed by agent identities, while NMD computes distances between behaviors $\pi \in \mathcal{B}$. This allows NMD to remain well-defined under the dynamics of our framework: behaviors that are transient, shared across agents, and adapted in response to events.

4.2 Architectural Realization

To capture, populate and navigate \mathcal{B} , we require an architecture satisfying three requirements: (i) it must produce behaviors as a function of an agent’s local observation and the most recent event; (ii) it must do so cheaply enough to avoid prohibitive per-timestep computation; and (iii) it must allow to introduce mechanisms to preserve the diversity of the behavior manifold \mathcal{B} . We achieve this with an event-driven hypernetwork that emits LoRA modules over a shared policy backbone.

Event-driven hypernetwork. Let g_θ be a transformer-based hypernetwork. Given the most recent event ξ_t , g_θ ingests a token per agent from their local observations $o_{i,t}$, the event encoding e_t , and the global target diversity scalar NMD_{des} , and emits a LoRA pair (C_m, D_m) per agent. Note that we use index m instead of i to highlight that the hypernetwork might predict the same (C_m, D_m) pair for various agents. The hypernetwork is queried only when an event fires (and once at initialization); between events, the pair is held fixed. This avoids the static brittleness of episode-initial generation [Tessera et al., 2025] and the cost and instability of per-step regeneration [Fu et al., 2025].

LoRA over a shared backbone. The team shares a policy backbone W_{shared} and applies the assigned LoRA adapters $D_m C_m$ to the final linear layer of the policy. Given the penultimate feature $\phi(o_t)$, the pre-activation output of behavior m is:

$$z_m(o_t) = W_{\text{shared}} \phi(o_t) + \alpha D_m C_m \phi(o_t), \quad (3)$$

where α is a scalar that is used to preserve diversity, which will be explained in Section 4.3. The final action distribution $\pi_m(o_t)$ is obtained by applying an activation function (squashed Gaussian for continuous control) to $z_m(o_t)$. Three design choices deserve note. First, restricting the hypernetwork to emit $C_m \in \mathbb{R}^{r \times d}$, $D_m \in \mathbb{R}^{d_a \times r}$ with $r \ll d$ stabilizes optimization relative to generating dense matrices; it also reduces the hypernetwork’s output dimensionality (see Appendix D.2). Second, applying the LoRA update to the final linear layer ensures that the heterogeneous component enters the policy linearly in $\phi(o_t)$, the condition that makes diversity maintenance possible and gradient projections analytically tractable (Section 4.3). Third, W_{shared} accumulates task-general representations, while (C_m, D_m) encodes only the deviation needed to instantiate a specific behavior, keeping the hypernetwork output small and the solution memory efficient. Overall, the event-based hypernetwork with LoRA modules allows us to learn a representation of \mathcal{B} through the weights θ of g_θ and, at the same time, assign behaviors to agents by generating (C_m, D_m) pairs, effectively allowing to capture, populate and navigate the behavior manifold \mathcal{B} .

4.3 Diversity Control on the Behavior Manifold

To ensure that the hypernetwork learns a well-structured behavior manifold, we opt to enforce a diversity constraint inspired by Diversity Control (DiCo) [Bettini et al., 2024a]. We express each behavior as the sum of a shared component $W_{\text{shared}} \phi(o_t)$ and a per-behavior deviation $u_m(o_t) = D_m C_m \phi(o_t)$, as described in Eq. (3). To ensure diversity constraint, the scalar α is set as:

$$\alpha = \frac{\text{NMD}_{\text{des}}}{\widehat{\text{NMD}}(\{u_m(o_t)\}_{m=1}^B)}, \quad (4)$$

where the denominator is computed over the B behaviors present in the parallel batch of environments, and NMD_{des} is the target diversity level. Because the LoRA update enters Eq. (3) linearly, scaling the deviations by α scales the resulting behavioral distance by α exactly, so the realized diversity equals NMD_{des} by construction. This linearity is the technical reason for the final-layer linear placement in Section 4.2: any nonlinearity between the LoRA update and the policy mean would forfeit this reduction. Our formulation is an extension of DiCo [Bettini et al., 2024a], which expresses each agent’s policy as $\pi_i(o) = \pi_h(o) + \lambda \pi_{h,i}(o)$, where π_h is a shared component, $\pi_{h,i}$ is a per-agent deviation, and λ scales the deviation to match a target SND value. However, unlike ours, DiCo is agent-centric: each $\pi_{h,i}$ is permanently bound to an agent and the matched diversity is measured between fixed agent indices. Together, Eqs. (3) and (4) generalize DiCo from a fixed set of indexed agents to the time-varying set of behaviors instantiated on the manifold.

This brings to the main result that justifies the architectural choice in Section 4.2 and the diversity control mechanism: we do not merely enforce a target diversity level, but also make reward optimization and diversity preservation jointly stable without auxiliary losses or trust regions.

Theorem 3. *The gradient of the expected return R with respect to the deviation $u_m(o_t)$ satisfies $\nabla_{u_m} R = \alpha P_{u_m} (\nabla_{z_m} R)^\top$, where $P_{u_m} = I - \frac{u_m \otimes \nabla_{u_m} \text{NMD}}{\text{NMD}}$ is an idempotent projection matrix.*

The theorem shows that diversity control does not enter as an external regularizer, but as a projector on the reward-maximizing gradient: any component of $\nabla_{z_m} R$ that would alter $\widehat{\text{NMD}}$ is filtered out before the LoRA parameters are updated. The reward objective and the diversity constraint are therefore aligned by construction—the optimized architecture can move freely along directions that preserve realized diversity, and is gated along directions that would violate it.

Corollary 4. *The projection P_{u_m} has two limiting regimes. **Vanishing deviation:** when $\|u_m\| \rightarrow 0$, $P_{u_m} \rightarrow I$ and the gradient is unprojected, allowing the behavior to escape a degenerate niche. **Dominant deviation:** when $\|u_m\|$ is large, P_{u_m} contracts strongly along u_m , suppressing updates that would further amplify $\|u_m\|$ and collapse the heterogeneity of the remaining behaviors.*

5 Experiments

We empirically address four questions. First, we assess whether our framework constitutes a competitive MARL approach: **(Q1) How does our framework perform relative to established baselines across benchmarks?** Second, if behaviors are truly properties of the task, our approach should generalize without retraining across agent counts and capabilities. Our constrained formulation further enables generalization to a third axis, target diversity levels: **(Q2) Does the framework generalize zero-shot across varying agent counts, capabilities, and diversity levels?** Third, we verify that our event-based framework triggers the intended behavioral shifts: **(Q3) Can our framework solve tasks that require sequential behavior allocation in response to events?** Fourth, if behaviors are task properties, the framework should also generalize to unseen event sequences, such as the removal of an agent mid-episode: **(Q4) Does our framework generalize to unseen event sequences?**

5.1 Experimental Setup

Baselines. We evaluate our framework against four baselines. **HyperMARL** [Tessera et al., 2025] allocates behaviors episode-wise via a hypernetwork conditioned on agent identities. Capability-Aware Shared Hypernetworks (**CASH**) [Fu et al., 2025] allocates behaviors at every timestep via a hypernetwork conditioned on capabilities when available, or agent identities. Diversity Control (**DiCo**) [Bettini et al., 2024a] inspired our constrained diversity optimization, but operates on fixed agent indices using cross-agent SND as the constraint; for each task, we perform a grid search over target SND values and report the best-performing variant. Finally, Parameter Sharing (**PS**) [Gupta et al., 2017] is a baseline with no behavior allocation, where all agents share the same policy.

Environments. We consider two sets of experiments. First, to address **(Q1)** and **(Q2)**, we evaluate our approach on four benchmarks established in recent studies on behavioral diversity [Tessera et al., 2025, Bettini et al., 2024a,b]: (i) **Navigation** (local-sensing exploration), (ii) **Dispersion** (reaching M targets from a central point), (iii) **Reverse Transport** (collective package pushing), and (iv) **Football** (competitive multi-team benchmark inspired by Google Research Football [Kurach et al., 2020]). Second, to address **(Q3)** and **(Q4)**, we introduce two custom tasks designed to highlight the benefits of our event-driven formulation. **Pressure Plate** requires a team to coordinate sequentially by holding down plates to open a locked door separating them from their goal; this task can only be solved with sequential event-based behavior allocation. **Wind Flocking** requires the team to maintain a formation where an agent must provide shielding for another agent against wind resistance; this task allows for direct visualization of the effects of our proposed NMD. All environments are implemented in VMAS [Bettini et al., 2022], a popular and scalable MARL simulator. Details are in Appendix C and source code at <https://anonymous.4open.science/r/hyperscale-48D6/>.

Events. A key dimension of our framework is the event. In our experiments, an event is defined by the removal of an agent, a modification in agent capabilities, a change in the target diversity, or a change in an element of the environment (e.g., door open). In tasks featuring partial observability, such as Navigation, a change in the local LiDAR reading is likewise categorized as an event.

5.2 Q1: Performance compared to establish baselines

To address **(Q1)**, we evaluate the performance of all approaches across the four primary tasks. Fig. 2 reports the task-specific completion rate, the average reward, and the episode length. Our proposed framework systematically ranks top-1, achieving a completion rate of at least 95% across all tasks and significantly outperforming all baselines on the more complex Football task.

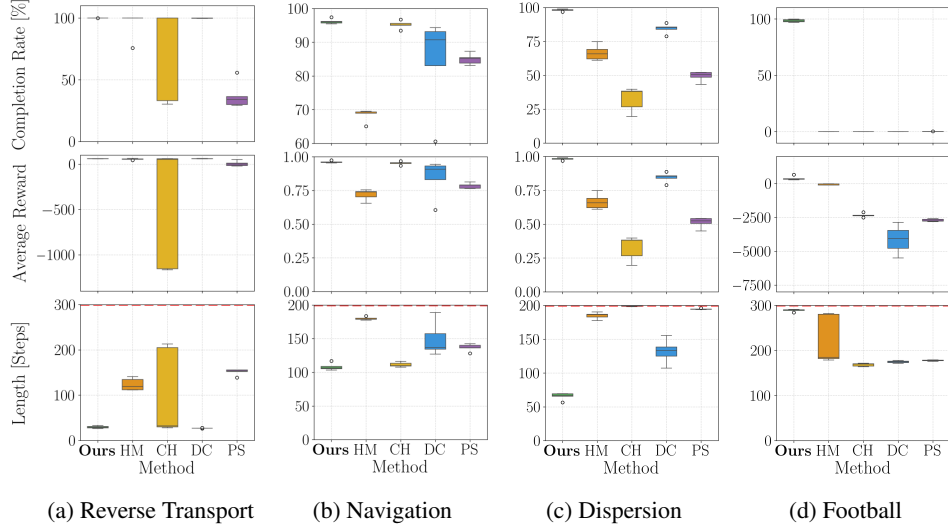


Figure 2: **Performance Comparison.** Final completion rate, average reward, and episode length across 5 seeds. Colors represent methods: green (Ours), orange (HM: HyperMARL), yellow (CH: CASH), blue (DC: DiCo), purple (PS: Parameter Sharing).

Examining each panel reveals how the performance gap scales with task complexity. On Reverse Transport, all methods reach competitive completion rates except **PS**. The clear separation in this task is in episode length, where our method consistently terminates earliest, closely followed by **DiCo** but with a wide gap with respect of the other methods. This indicates that event-driven behavior allocation produces more direct trajectories rather than merely succeeding more often. On Navigation, only our framework and **CASH** reach high completion with low episode length. On Dispersion, the gap widens. Our framework retains a near-perfect completion rate while **CASH** drops to roughly 50%, **DiCo** to roughly 80%, and **HyperMARL** and **PS** collapse. This is the first task where static behavior assignment becomes a clear liability: with M targets and no per-target specialization unlocked at the right moment, agents converge on overlapping subsets of targets. The most pronounced gap appears on Football, where every baseline collapses to near-zero completion, while our framework remains close to 100%. We attribute this to the task’s reliance on event-driven role transitions—possession changes, ball proximity, opponent positioning—which static or scheduled allocations cannot track.

5.3 Q2: Zero-shot Generalization across Number of Agents, Capabilities and Target Diversity

To address (Q2), we evaluate generalization across three axes. For agent count generalization, we exclude **HyperMARL** as its architecture cannot accommodate changes in team size, and replicate learned policies for **DiCo** and **PS** to enable comparison. For capability generalization, the considered tasks are homogeneous by default, so we run independent training runs for multiple capability values, concatenating capabilities to observations as inputs to the hypernetworks for our framework and **CASH**. The varied capabilities are: LiDAR range for Navigation, agent speed for Dispersion and Football, and agent force for Reverse Transport. Diversity target generalization is enabled directly by our constrained formulation and requires no additional training runs.

The results in Fig. 3 show that our proposed approach maintains performance across these axes of zero-shot generalization, while baselines either stagnate or lose performance. Along the agent-count axis, our framework remains stable across the entire in-distribution and out-distribution ranges for all tasks, evidence that the hypernetwork has learned a behavior manifold in which changing the number of agents simply implies sampling a different amount of points in \mathcal{B} . The same conclusion can be drawn from the capability axis. Variations in LiDAR range, agent speed, and pushing force leave the high completion rate of our method largely unchanged, consistently outperforming baselines.

Along the target NMD axis, our completion rate is stable across roughly two order of magnitude of NMD values. Interestingly, the absolute value of these ranges vary across tasks, which implies that there is actually a “good” region of NMD values. The stability of this last axis is the empirical

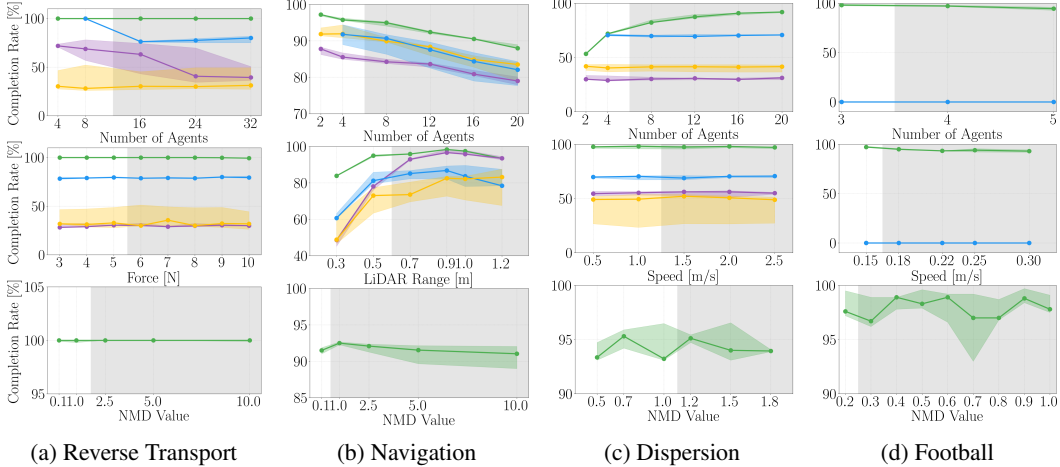


Figure 3: **Generalization.** Final completion rate across 5 seeds for the three generalization axes. White areas denote training distribution; gray areas denote zero-shot evaluation. Colors represent methods: green (Ours), yellow (CH: CASH), blue (DC: DiCo), purple (PS: Parameter Sharing).

counterpart to Theorem 3: because diversity is enforced through a projection, the achievable reward does not change as NMD_{des} is varied within reasonable ranges. Overall, this also helps to explain the success of our approach, as diversity control maintains a sufficient level of diversity to span all necessary behaviors to solve the task.

5.4 Q3: Adaptive Behaviors in Response to Events

To address (Q3), we introduce the Pressure Plate task, which requires accurate event-based behavior allocation to succeed. In this scenario, agents must adopt multiple behaviors sequentially; for example, one agent must hold a pressure plate until teammates pass through a door, then transition to a new behavior once a second plate is secured on the opposite side. The results in Fig. 4a and 4b show that our approach is the only evaluated method that successfully completes the task.

To verify that this performance is driven by the event mechanism, we compare our approach to an ablation without event re-querying. This ablation fails because agents are statically assigned a single behavior, leaving them unable to adapt to the sequential requirements of the task, which results in the final agent remaining stuck behind the door. Interestingly, our event-based formulation enables sequential strategies without explicit time awareness, an emergent property from the decoupling of agent identity and behavior. This is further studied in Fig. 1, that visualizes agent trajectories and a t-SNE projection of the behavior space \mathcal{B} . Across multiple stochastic runs, distinct clusters emerge, demonstrating that event-based re-querying induces specialized and consistent behavioral modes.

5.5 Q4: Generalization to Unseen Event Sequences

To address (Q4), we evaluate the Football, Pressure Plate, and Wind Flocking environments by introducing unseen event sequences. Specifically, in Football, we remove an agent at a random point; in Pressure Plate, we remove the agent that first reaches the second pressure plate; and in Wind Flocking, we randomly change the target diversity mid-episode. Results in Table 4c demonstrate that our method is robust to these additional events and successfully recovers, highlighting its ability to assign relevant behaviors following such events. Specifically, neither perturbation pushes performance into the regime occupied by the baselines in Section 5.2, suggesting that the framework’s response to unseen events is qualitatively close to redistributing roles.

Fig. 4d visualizes the impact of diversity on the Wind Flocking environment: as the requested diversity decreases, the agents form tighter flocks, highlighting the direct effect of NMD on agent behavior. The four snapshots correspond to NMD targets that change mid-episode. The agent geometry tracks each change visibly: the inter-agent distance grows monotonically with NMD between steps 20 and 120, and contracts again at step 170 once NMD is reduced below the initial value. Because the target

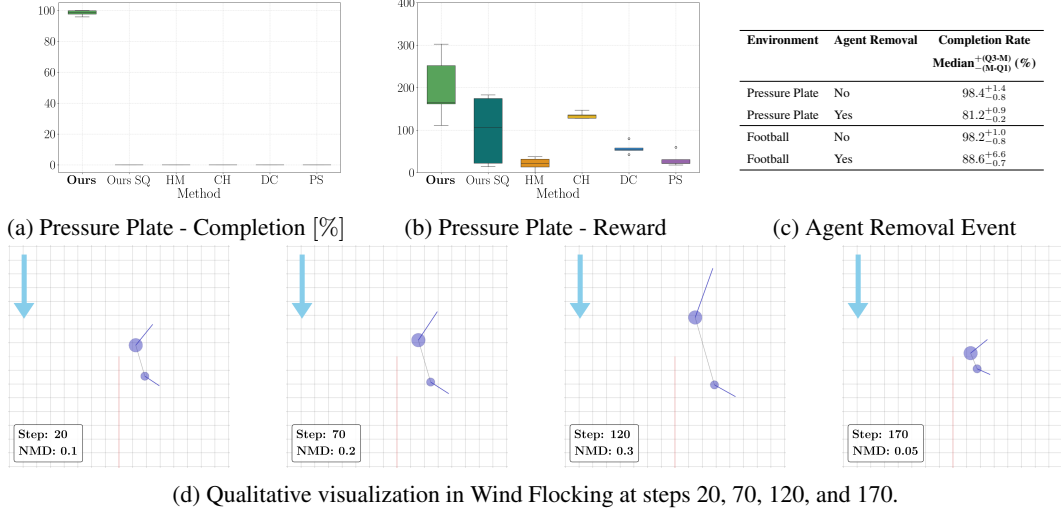


Figure 4: **Study of Events.** (a) Completion rate and (b) average episode reward on Pressure Plate. Colors: green (Ours and SQ: Single Query), orange (HM: HyperMARL), yellow (CH: CASH), blue (DC: DiCo), purple (PS: Parameter Sharing). (c) Agent removal on Pressure Plate and Football. (d) Visualization for four NMD values in Wind Flocking. The arrow indicates wind direction.

diversity is supplied to the hypernetwork as an input scalar, this transition does not require retraining and confirms that NMD_{des} acts as a direct, interpretable control on the realized formation rather than as a soft regularization target. Quantitative results are reported in Appendix D.1.

6 Conclusion, Limitations, and Future Work

This work argues that behavioral adaptation in MARL is best understood as event-driven: triggered by task-relevant transitions rather than by agent identity or fixed temporal cadence. From this premise follows a structural decoupling in which behaviors are no longer tied to agents but instantiated from a continuous manifold the team shares. As a consequence, the meaning of diversity is shifted to a property of the task, not of the agents that populate it. We made this concrete through Neural Manifold Diversity, which we proved is a valid distance on behaviors, and through an event-driven hypernetwork that generates LoRA modules over a shared policy. We also proved that this implementation aligns reward maximization with diversity preservation by design. Our empirical results demonstrated that our framework facilitates more effective coordination and generalization compared to existing approaches, outperforming baselines. The benefits of an event-based formulation are further validated in a pressure plate task, in which sequential assignment emerges to solve the task despite the absence of a memory mechanism (e.g., RNN) that learns a state-machine representation of the task status.

Although this work establishes the foundation for an event-based view of behavioral adaptation in MARL, it presents limitations. The societal implications of these are discussed Appendix E, while here we focus on the technical limitations. First, the expressivity of behaviors is inherently constrained by the choice of representation. We use an implicit behavior typing representation where behaviors are inferred from local observations and attention to teammate observations via a hypernetwork, which results in diversity expressed within the space of policy parameters. Consequently, the richness of the strategy space is tied to this specific representation. As an initial effort to investigate this constraint, we provide experiments regarding the dimensionality of our LoRA adapter in Appendix D.2. Second, we note that in our current formulation, events are defined a priori using domain knowledge. A compelling extension for future work involves inferring these events either end-to-end or through latent discovery. This logic similarly applies to the diversity target, as our method generalizes across a range of NMD values, yet the identification of optimal values for this metric could likely be automated through an additional optimization objective. Lastly, the realization of our framework through a hypernetwork is currently centralized, requiring access to the observations from all agents to assign behaviors. It would be interesting to derive an extension of our solution that is decentralized, in which agents decide on their behavior based only on neighboring information.

Acknowledgements

This work is supported by the European Research Council (ERC) Project 949940 (gAIa), by a Leverhulme Trust Research Project Grant, and by the EPSRC funded INFORMED-AI project EP/Y028732/1. We gratefully acknowledge their support.

References

- Matteo Bettini, Ryan Kortvelesy, Jan Blumenkamp, and Amanda Prorok. VMAS: A vectorized multi-agent simulator for collective robot learning. In *International Symposium on Distributed Autonomous Robotic Systems*, pages 42–56. Springer, 2022.
- Matteo Bettini, Ajay Shankar, and Amanda Prorok. Heterogeneous multi-robot reinforcement learning. In *International Conference on Autonomous Agents and Multiagent Systems*, pages 1485–1494. International Foundation for Autonomous Agents and Multiagent Systems, 2023.
- Matteo Bettini, Ryan Kortvelesy, and Amanda Prorok. Controlling behavioral diversity in multi-agent reinforcement learning. In *International Conference on Machine Learning*, pages 3611–3636, 2024a.
- Matteo Bettini, Ryan Kortvelesy, and Amanda Prorok. The impact of behavioral diversity in multi-agent reinforcement learning. *arXiv preprint arXiv:2412.16244*, 2024b.
- Matteo Bettini, Ajay Shankar, and Amanda Prorok. System Neural Diversity: Measuring Behavioral Heterogeneity in Multi-Agent Learning. *Journal of Machine Learning Research*, 26(163):1–27, 2025.
- Filippos Christianos, Georgios Papoudakis, Muhammad A Rahman, and Stefano V Albrecht. Scaling multi-agent reinforcement learning with selective parameter sharing. In *International Conference on Machine Learning*, pages 1989–1998. PMLR, 2021.
- Ankur Deka and Katia Sycara. Natural emergence of heterogeneous strategies in artificially intelligent competitive teams. In *International Conference on Swarm Intelligence*, pages 13–25. Springer, 2021.
- Kevin Fu, Shalin Jain, Pierce Howell, and Harish Ravichandar. Capability-aware shared hypernetworks for flexible heterogeneous multi-robot coordination. In *Conference on Robot Learning*, pages 1576–1597. PMLR, 2025.
- Harsh Goel, Mohammad Omama, Behdad Chalaki, Vaishnav Tadiparthi, Ehsan Moradi Pari, and Sandeep P Chinchali. R3DM: Enabling role discovery and diversity through dynamics models in multi-agent reinforcement learning. In *International Conference on Machine Learning*, pages 19600–19620. PMLR, 2025.
- Jayesh K Gupta, Maxim Egorov, and Mykel Kochenderfer. Cooperative multi-agent control using deep reinforcement learning. In *International Conference on Autonomous Agents and Multiagent Systems*, pages 66–83. Springer, 2017.
- Edward J Hu, Yelong Shen, Phillip Wallis, Zeyuan Allen-Zhu, Yuanzhi Li, Shean Wang, Liang Wang, Weizhu Chen, et al. Lora: Low-rank adaptation of large language models. *International Conference on Learning Representations*, 1(2):3, 2022.
- Jiechuan Jiang and Zongqing Lu. The emergence of individuality. In *International Conference on Machine Learning*, pages 4992–5001. PMLR, 2021.
- Woojun Kim and Younghul Sung. Parameter sharing with network pruning for scalable multi-agent deep reinforcement learning. In *International Conference on Autonomous Agents and Multiagent Systems*, pages 1942–1950, 2023.
- Karol Kurach, Anton Raichuk, Piotr Stańczyk, Michał Zajac, Olivier Bachem, Lasse Espeholt, Carlos Riquelme, Damien Vincent, Marcin Michalski, Olivier Bousquet, et al. Google research football: A novel reinforcement learning environment. In *AAAI Conference on Artificial Intelligence*, volume 34, pages 4501–4510, 2020.

- Chenghao Li, Tonghan Wang, Chengjie Wu, Qianchuan Zhao, Jun Yang, and Chongjie Zhang. Celebrating diversity in shared multi-agent reinforcement learning. *Advances in Neural Information Processing Systems*, 34:3991–4002, 2021.
- Dapeng Li, Na Lou, Bin Zhang, Zhiwei Xu, and Guoliang Fan. Adaptive parameter sharing for multi-agent reinforcement learning. In *IEEE International Conference on Acoustics, Speech and Signal Processing*, pages 6035–6039, 2024.
- Yirui Liu. Dynamic Role Learning in Multi-Agent Reinforcement Learning: Hypernetwork-Based Agent Net with Contrastive Learning Representations. In *International Conference on Artificial Intelligence, Automation and High Performance Computing*, pages 650–654, 2025.
- Anuj Mahajan, Tabish Rashid, Mikayel Samvelyan, and Shimon Whiteson. Maven: Multi-agent variational exploration. *Advances in Neural Information Processing Systems*, 32, 2019.
- Ingram Olkin and Friedrich Pukelsheim. The distance between two random vectors with given dispersion matrices. *Linear Algebra and its Applications*, 48:257–263, 1982.
- Hanwen Qi, Tinghuai Ma, Kexing Peng, and Xin Yu. Rois: Role-based multi-agent collaboration by context-time-aware information sharing. *ACM Transactions on Intelligent Systems and Technology*, 17(1):1–27, 2026.
- L. S. Shapley. Stochastic Games. *Proceedings of the National Academy of Sciences*, 39(10):1095–1100, 1953.
- Mingxi Tan, Andong Tian, and Ludovic Denoyer. Policy diversity for cooperative agents. In *IEEE Conference on Games*, pages 1–4, 2023.
- Kale-ab Abebe Tessler, Arrasy Rahman, Amos Storkey, and Stefano V Albrecht. HyperMARRL: Adaptive hypernetworks for multi-agent rl. In *Advances in Neural Information Processing Systems*, 2025.
- Cédric Villani et al. *Optimal transport: old and new*, volume 338. Springer, 2009.
- Tonghan Wang, Heng Dong, Victor Lesser, and Chongjie Zhang. ROMA: multi-agent reinforcement learning with emergent roles. In *International Conference on Machine Learning*, pages 9876–9886, 2020a.
- Tonghan Wang, Tarun Gupta, Anuj Mahajan, Bei Peng, Shimon Whiteson, and Chongjie Zhang. RODE: Learning roles to decompose multi-agent tasks. In *International Conference on Learning Representations*, 2020b.

A Extended Related Work

Temporal Behavioral Assignment. A core question for behavior allocation is the assignment timeline. Existing approaches fall into two categories. The first one comprises methods that fix one behavior per agent for the entire episode [Tessler et al., 2025, Bettini et al., 2024a, Jiang and Lu, 2021, Li et al., 2021, Liu, 2025, Christianos et al., 2021], either because they learn per-agent policies [Bettini et al., 2024a, Jiang and Lu, 2021, Christianos et al., 2021], or because they do not allow dynamically changing behavior [Tessler et al., 2025, Li et al., 2021, Liu, 2025]. The second category comprises methods that adapt behaviors on a fixed temporal schedule—either every timestep or every c steps—regardless of task conditions [Fu et al., 2025, Qi et al., 2026, Mahajan et al., 2019, Wang et al., 2020a,b, Goel et al., 2025].

Representations of Behaviors. Behavioral specialization is fundamentally constrained by the underlying behavior representation. A common paradigm is to learn explicit policies for each behavior, with methodologies ranging from learning deviations from a common policy [Li et al., 2021, Bettini et al., 2024a] to selective parameter sharing [Christianos et al., 2021, Kim and Sung, 2023, Li et al., 2024, Jiang and Lu, 2021]. However, these approaches do not easily accommodate dynamic behavior allocation as the learned behaviors remain fixed and tied to specific agents. Another

frequent approach is to use a shared policy conditioned on agent identity, typically defined as one-hot encoding [Tessera et al., 2025], or capabilities when available [Fu et al., 2025]. This method, also known as behavior typing [Bettini et al., 2023], has been applied through both direct policy conditioning [Deka and Sycara, 2021] and conditioned hypernetworks that indirectly predict policy parameters [Tessera et al., 2025, Fu et al., 2025]. However, it inherently limits scalability. A more flexible extension involves learning a latent behavior space (or role space) from which behaviors are sampled, either to condition a shared policy [Mahajan et al., 2019, Qi et al., 2026, Goel et al., 2025] or a shared hypernetwork [Wang et al., 2020a, Liu, 2025]. While this has shown promising results, it relies on training additional encoder networks and requires prior knowledge on the dimensionality and structure of the latent space to identify distinct behaviors. Alternatively, Wang et al. [2020b] achieves specialization by partitioning the action space, though this requires fixing the decomposition early to maintain tractability. In contrast to these explicitly conditioned or constrained methods, inferred behavior typing [Gupta et al., 2017, Bettini et al., 2023] derives behavior solely from environmental observations.

Quantifying and Enforcing Behavioral Diversity. While the previous section focuses on enabling diversity through representation, this is often insufficient to ensure functional divergence in practice. Consequently, while some works do not explicitly reward diversity [Wang et al., 2020b, Christianos et al., 2021], many works have proposed various methods to encourage diversity within teams. These methods generally fall into two categories: those that encourage diversity through auxiliary rewards or losses [Wang et al., 2020a, Li et al., 2021, Mahajan et al., 2019, Jiang and Lu, 2021, Liu, 2025, Qi et al., 2026, Goel et al., 2025], and those that enforce diversity as a constraint in the learning process [Bettini et al., 2024a, Tan et al., 2023]. While the first type of approach is easier to construct and optimize, it offers only weak guarantees on final team diversity. The second type provides a strong guarantee that diversity constraints will be satisfied, although it requires a reference target value to be known a priori. Additionally, researchers have proposed different ways to quantify this diversity. Many papers focus on information-theoretic objectives where the trajectories of a policy should carry maximum information about its behavior [Wang et al., 2020a, Li et al., 2021, Mahajan et al., 2019, Jiang and Lu, 2021, Qi et al., 2026, Goel et al., 2025], requiring training models to differentiate trajectories. Alternatively, [Liu, 2025] proposes to use a contrastive loss to distinguish behavior, which also requires a separate model to differentiate trajectories. Finally, Bettini et al. [2025] proposed System Neural Diversity (SND), an explicit diversity metric based on the action distribution of the policies.

B Proofs of Theoretical Results

B.1 Notation and Assumptions

(A1) Behavior manifold. The behavior manifold \mathcal{B} is a measurable space of conditional action distributions $\pi : \mathcal{O} \rightarrow \mathcal{P}(\mathcal{A})$, where $\mathcal{P}(\mathcal{A})$ denotes the set of Borel probability measures on the action space \mathcal{A} . We assume $\mathcal{A} \subseteq \mathbb{R}^{d_a}$ is equipped with the Euclidean norm $\|\cdot\|$, and that for every $\pi \in \mathcal{B}$ and every $o \in \mathcal{O}$, the action distribution $\pi(o)$ has finite second moment.

(A2) Observation distribution. Observations $o \in \mathcal{O}$ are drawn from a probability density $p(o)$, and behaviors $\pi \in \mathcal{B}$ are drawn from a density $p(\pi)$. All integrals over \mathcal{O} and \mathcal{B} are taken with respect to these densities.

(A3) Gaussian policy parameterization. When invoked (Lemma 6 onward), each behavior π_m is a Gaussian policy $\pi_m(\cdot | o) = \mathcal{N}(\mu_m(o), \Sigma)$, with mean $\mu_m(o) \in \mathbb{R}^{d_a}$ and a covariance $\Sigma \succ 0$ that is shared across behaviors and independent of o .

(A4) Linear LoRA parameterization. The mean of behavior m is decomposed as $\mu_m(o) = W_{\text{shared}} \phi(o) + \alpha u_m(o)$, $u_m(o) := D_m C_m \phi(o)$, where $\phi(o) \in \mathbb{R}^d$ is a shared feature, $W_{\text{shared}} \in \mathbb{R}^{d_a \times d}$ is the shared backbone, $C_m \in \mathbb{R}^{r \times d}$ and $D_m \in \mathbb{R}^{d_a \times r}$ are the LoRA factors, and $\alpha \in \mathbb{R}_{>0}$ is the diversity scalar. The deviation $u_m(o)$ is deterministic.

(A5) Differentiability. The expected return R is differentiable in the LoRA parameters $\{C_m, D_m\}$ and in the shared parameters via ϕ and W_{shared} , and the empirical NMD estimator $\widehat{\text{NMD}}$ defined in Eq. (2) of the main text is differentiable in the deviations $\{u_m\}$ on the open set $\widehat{\text{NMD}} > 0$. For

a fixed observation o , we abbreviate $u_m := u_m(o)$, $\mu_m := \mu_m(o)$, $\phi := \phi(o)$, and $z_m := \mu_m$ (the policy mean coincides with the pre-activation in (A3)–(A4)).

B.2 Proof of Proposition 2

Proof. We verify the four metric axioms.

Non-negativity. For every o , the 2-Wasserstein distance satisfies $W_2(\pi_m(o), \pi_n(o)) \geq 0$ (it is a metric on $\mathcal{P}_2(\mathcal{A})$ by [Villani et al., 2009] Thm. 6.18). The expectation of a non-negative integrand is non-negative, so $d(\pi_m, \pi_n) \geq 0$.

Symmetry. W_2 is symmetric in its arguments, hence $W_2(\pi_m(o), \pi_n(o)) = W_2(\pi_n(o), \pi_m(o))$ point-wise in o , and the expectation preserves equality.

Triangle inequality. Fix any $\pi_m, \pi_n, \pi_k \in \mathcal{B}$. Point-wise in o , the triangle inequality for W_2 gives

$$W_2(\pi_m(o), \pi_k(o)) \leq W_2(\pi_m(o), \pi_n(o)) + W_2(\pi_n(o), \pi_k(o)).$$

Taking expectation under $p(o)$ and using linearity and monotonicity of expectation:

$$d(\pi_m, \pi_k) \leq d(\pi_m, \pi_n) + d(\pi_n, \pi_k).$$

Identity. If $\pi_m = \pi_n$ in \mathcal{B} , then $\pi_m(o) = \pi_n(o)$ for all o , hence $W_2(\pi_m(o), \pi_n(o)) = 0$ point-wise and $d(\pi_m, \pi_n) = 0$. Conversely, $d(\pi_m, \pi_n) = 0$ implies $W_2(\pi_m(o), \pi_n(o)) = 0$ for p -almost every o , hence $\pi_m(o) = \pi_n(o)$ for p -almost every o . This gives identity up to p -null sets, which establishes the pseudometric property. Under the additional separation assumption the converse is strengthened to $\pi_m = \pi_n$, yielding a genuine metric. \square

Corollary 5. *Under the separation assumption, $\text{NMD}(\mathcal{B}) = 0$ if and only if $p(\pi)$ concentrates on a single behavior. The forward direction follows from $d(\pi_m, \pi_n) = 0 \iff \pi_m = \pi_n$; the converse from non-negativity of d and the integral definition of NMD.*

B.3 Proof of Theorem 3

Before proving the main result of the theorem, we state and prove a Lemma that helps to derive the connection between diversity in the behavior manifold and reward maximization.

Lemma 6. *Let π_m be a Gaussian policy with mean μ_m and covariance Σ shared across behaviors. If the heterogeneous component $u_m(o_t)$ enters μ_m linearly and is deterministic, then $W_2(\pi_m, \pi_n) = \|\mu_m - \mu_n\|_2$.*

Proof. The closed-form expression for the 2-Wasserstein distance between two non-degenerate Gaussians on \mathbb{R}^{d_a} is

$$W_2^2(\mathcal{N}(\mu_m, \Sigma_m), \mathcal{N}(\mu_n, \Sigma_n)) = \|\mu_m - \mu_n\|_2^2 + \text{tr}\left(\Sigma_m + \Sigma_n - 2(\Sigma_m^{1/2}\Sigma_n\Sigma_m^{1/2})^{1/2}\right),$$

a result due to Olkin and Pukelsheim [1982]. Under (A3), $\Sigma_m = \Sigma_n = \Sigma$, so

$$\Sigma_m + \Sigma_n - 2(\Sigma_m^{1/2}\Sigma_n\Sigma_m^{1/2})^{1/2} = 2\Sigma - 2(\Sigma^{1/2}\Sigma\Sigma^{1/2})^{1/2} = 2\Sigma - 2\Sigma = 0,$$

where we used that for $\Sigma \succ 0$, $\Sigma^{1/2}\Sigma\Sigma^{1/2} = \Sigma^2$ and $(\Sigma^2)^{1/2} = \Sigma$. The trace term vanishes, leaving

$$W_2^2(\pi_m(o), \pi_n(o)) = \|\mu_m(o) - \mu_n(o)\|_2^2.$$

Taking square roots (both sides are non-negative) gives the claim. \square

Substituting Lemma 2 into Eq. (2) of the main text and using $\mu_m(o) - \mu_n(o) = \alpha(u_m - u_n)$ from (A4), we obtain

$$\widehat{\text{NMD}}(\{\pi_m\}_{i=1}^b) = \frac{2\alpha}{b(b-1)|\mathcal{O}_{\text{ep}}|} \sum_{i < j} \sum_{o \in \mathcal{O}_{\text{ep}}} \|u_m - u_n\|_2. \quad (5)$$

This makes explicit that $\widehat{\text{NMD}}$ is a homogeneous function of degree 1 in the deviations $\{u_m\}$, result that leads to the proof of Theorem 3.

Proof. We compute $\nabla_{u_m} R$ via the chain rule, treating α as a function of $\{u_n\}_{j=1}^b$ through Eq. (5).

Step 1. From (A4), $z_m = W_{\text{shared}}\phi + \alpha u_m$. The dependence of z_m on u_m has two contributions: the explicit αu_m term, and the implicit dependence of α on u_m through $\widehat{\text{NMD}}$. Treating u_m as a vector in \mathbb{R}^{d_a} :

$$\frac{\partial z_m}{\partial u_m} = \alpha I + u_m \otimes \nabla_{u_m} \alpha,$$

where \otimes denotes the outer product (we use the convention $(a \otimes b)v = a(b^\top v)$). Substituting $\alpha = \text{NMD}_{\text{des}}/\widehat{\text{NMD}}$ and applying the quotient rule:

$$\nabla_{u_m} \alpha = -\frac{\text{NMD}_{\text{des}}}{\widehat{\text{NMD}}^2} \nabla_{u_m} \widehat{\text{NMD}} = -\frac{\alpha}{\widehat{\text{NMD}}} \nabla_{u_m} \widehat{\text{NMD}}.$$

Therefore,

$$\frac{\partial z_m}{\partial u_m} = \alpha I - \frac{\alpha}{\widehat{\text{NMD}}} u_m \otimes \nabla_{u_m} \widehat{\text{NMD}} = \alpha P_{u_m},$$

with P_{u_m} as in Theorem 3.

Step 2. By the chain rule,

$$\nabla_{u_m} R = \left(\frac{\partial z_m}{\partial u_m} \right)^\top \nabla_{z_m} R = \alpha P_{u_m}^\top \nabla_{z_m} R.$$

Because P_{u_m} is symmetric in the dyadic structure that matters for the projection identity below (we verify idempotency on the same form), we drop the transpose for notational convenience and write

$$\nabla_{u_m} R = \alpha P_{u_m} \nabla_{z_m} R.$$

Step 3. Using Eq. (5), $\widehat{\text{NMD}}_0$ is positively homogeneous of degree 1 in u_m . By Euler's homogeneous function theorem,

$$u_m^\top \nabla_{u_m} \widehat{\text{NMD}} = \widehat{\text{NMD}}. \quad (6)$$

Now compute $P_{u_m}^2$. Writing $v := \nabla_{u_m} \widehat{\text{NMD}}$ and $N := \widehat{\text{NMD}}$ for brevity,

$$P_{u_m}^2 = \left(I - \frac{u_m v^\top}{N} \right) \left(I - \frac{u_m v^\top}{N} \right) = I - \frac{2 u_m v^\top}{N} + \frac{u_m (v^\top u_m) v^\top}{N^2}.$$

By Eq. (6), $v^\top u_m = N$, so the last term simplifies:

$$\frac{u_m (v^\top u_m) v^\top}{N^2} = \frac{u_m N v^\top}{N^2} = \frac{u_m v^\top}{N}.$$

Substituting back,

$$P_{u_m}^2 = I - \frac{2 u_m v^\top}{N} + \frac{u_m v^\top}{N} = I - \frac{u_m v^\top}{N} = P_{u_m}.$$

Thus P_{u_m} is idempotent. \square

B.4 Proof of Corollary 4

Proof. (i) The empirical NMD is the symmetric pairwise sum (Eq. (5))

$$\widehat{\text{NMD}} \propto \sum_{j \neq k} \|u_j - u_k\|_2 / [\text{normalization}].$$

Differentiating with respect to u_m :

$$\nabla_{u_m} \widehat{\text{NMD}} = c \sum_{j \neq i} \frac{u_m - u_n}{\|u_m - u_n\|_2},$$

for a positive constant c depending only on B and $|\mathcal{O}_{\text{ep}}|$. As $\|u_m\| \rightarrow 0$ (with all $\|u_n\|$ for $j \neq i$ bounded away from zero), the summand vectors $(u_m - u_n)/\|u_m - u_n\|_2$ remain bounded in norm

by 1, but the second-moment contribution to P_{u_m} is the rank-one term $u_m \otimes \nabla_{u_m} \widehat{\text{NMD}} / \widehat{\text{NMD}}$. The numerator factor $u_m \rightarrow 0$ drives this rank-one term to zero in operator norm, while the denominator $\widehat{\text{NMD}}$ remains bounded below by a positive constant (since the remaining behaviors maintain non-trivial pairwise distances). Hence $P_{u_m} \rightarrow I$.

(ii) Write $u_m = t\hat{u}_m$ with $t \rightarrow \infty$ and \hat{u}_m fixed. For large t , the dominant pairs (u_m, u_n) in $\widehat{\text{NMD}}$ are those involving u_m , since $\|u_m - u_n\| \sim t$ while $\|u_n - u_k\|$ for $j, k \neq i$ remains $O(1)$. Asymptotically,

$$\widehat{\text{NMD}} = \frac{c(B-1)}{B(B-1)/2} t + O(1) = \frac{2c}{B} t + O(1),$$

and

$$\nabla_{u_m} \widehat{\text{NMD}} = c \sum_{j \neq i} \frac{u_m - u_n}{\|u_m - u_n\|_2} = c(B-1) \hat{u}_m + O(1/t).$$

Substituting into the expression for P_{u_m} in Theorem 3 and using $u_m = t\hat{u}_m$:

$$P_{u_m} = I - \frac{(t\hat{u}_m)(c(B-1)\hat{u}_m + O(1/t))^\top}{(2c/B)t + O(1)} = I - \frac{c(B-1)t\hat{u}_m\hat{u}_m^\top}{(2c/B)t} + O(1/t).$$

Canceling t in the leading term:

$$P_{u_m} \rightarrow I - \frac{B(B-1)}{2} \hat{u}_m\hat{u}_m^\top \quad \text{as } t \rightarrow \infty.$$

This is the orthogonal projector onto \hat{u}_m^\perp . □

B.5 Bounded Action Spaces and Saturated Activations

Lemma 6 assumes a Gaussian policy with linear mean. In practice, continuous-control policies typically apply a squashing nonlinearity such as \tanh to enforce bounded actions, yielding $a = \tanh(z)$ with $z \sim \mathcal{N}(\mu, \Sigma)$. We discuss the impact on the preceding results.

Effect on Lemma 6. The Wasserstein distance between two squashed Gaussians no longer admits a closed form: the push-forward of a Gaussian under \tanh is non-Gaussian, and W_2 between such distributions must be computed numerically. However, in the unsaturated regime a standard Lipschitz inequality gives

$$W_2(\pi_m \circ \tanh^{-1}, \pi_n \circ \tanh^{-1}) \leq L_{\tanh} W_2(\pi_m, \pi_n) = L_{\tanh} \|\mu_m - \mu_n\|_2,$$

with $L_{\tanh} = 1$. NMD computed in pre-activation space therefore upper-bounds NMD computed in action space, and the relative ordering of behaviors is preserved.

Effect on Theorem 3. The chain rule of Step 1 acquires an extra Jacobian factor $\text{diag}(\text{sech}^2(z_m))$. In the unsaturated regime this Jacobian is close to the identity and the projection structure of P_{u_m} is preserved with multiplicative error $O(\|z_m\|^2)$. In the saturated regime the gradient flow $\nabla_{z_m} R$ along those coordinates is suppressed by the activation rather than the projector, so the projection P_{u_m} contributes no further regulation in those directions. The corollary’s qualitative regimes (vanishing/dominant deviation) carry over coordinate-wise, with the saturation acting as an additional, complementary gating mechanism rather than as a violation of the analysis.

Effect on Corollary 4. Vanishing-deviation behavior (regime (i)) is unaffected, since $\mu_m \rightarrow W_{\text{shared}}\phi$ remains in the unsaturated regime for typical feature scales. Dominant-deviation behavior (regime (ii)) is strengthened: as $\|u_m\| \rightarrow \infty$, the squashing nonlinearity contributes additional suppression on top of the projector, ensuring that pathologically large LoRA outputs cannot escape regulation through the action nonlinearity.

C Experimental Details

We evaluate our approach across six distinct multi-agent tasks that challenge various aspects of coordination, observability, and physical interaction.

Dispersion: all agents spawn at the center of the arena while goals are distributed randomly. The complexity lies in the fact that with total observability and a shared starting point, agents must

coordinate to ensure they do not all converge to the same closest goal. The optimal policy requires high behavioral diversity to disperse and tackle different goals simultaneously (Fig. 5a).

Navigation: introduces limited observability, requiring agents to utilize LiDAR sensors to explore the area and locate specific goals. Agents must navigate efficiently under time constraints, relying on LiDAR to locate their specific targets in an environment where information is sparse during the initial exploration phase (Fig. 5b).

Reverse Transport: agents spawn inside a physical package and must exert collective force to push it toward a goal. Because one agent is barely able to move the mass alone, the team must synchronize their velocities to move the package effectively, receiving rewards proportional to the reduction in distance to the goal (Fig. 5c).

Football: features a team of three agents playing against a programmed heuristic. Beyond coordinating an attack to score a goal (sparse reward), the random spawn locations force agents to switch between defensive positioning and counter-attacking. The challenge is amplified by the need to manage ball control and shooting lanes while competing against a consistent heuristic opponent (Fig. 5d).

Pressure Plate: a logic-based task where three agents must navigate a locked door by utilizing two pressure plates. This necessitates a three-phase strategy: (i) one agent presses the first plate to allow the others to cross, (ii) those agents must then find and hold a second plate on the opposite side so the first agent can also cross, and (iii) all agents move to the final goal (Fig. 5e).

Wind Flocking: explores energy-efficient collective movement among heterogeneous agents exposed to a north-to-south wind. The agents must discover a formation where the larger agent shields the smaller one from the wind to optimize their performance and minimize energy expenditure (Fig. 5f).

For initial experimentation, we required around 500 compute hours using an NVIDIA GeForce RTX 2080 Ti GPU and an Intel(R) Xeon(R) Gold 6248R CPU @ 3.00GHz. For the final multi-seed evaluation, we invested additional 500 compute hours on the same hardware. All the hyperparameters used in the paper can be found in Table 1.

D More Results

D.1 Average Episode Rewards for Main Experiments

For all reported results in the main text, we evaluated the models using the best-performing checkpoints saved during the training process. Fig. 6 illustrates the learning progress across our six evaluation environments: Navigation, Dispersion, Reverse Transport, Football, Pressure Plate, and Wind Flocking. The plots compare our method against the four baselines:

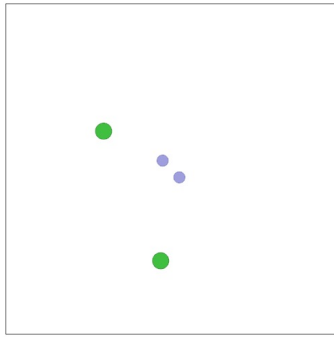
Full Parameter-Sharing. A homogeneous baseline with no behavior allocation, where all agents share the same policy.

HyperMARL [Tessera et al., 2025]. Allocates behaviors episode-wise at timestep 0 via a hypernetwork conditioned on agent identities.

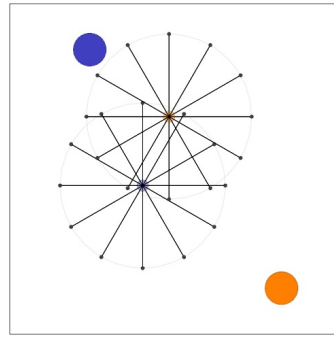
Diversity Control (DiCo) [Bettini et al., 2024a] Operates on fixed agent indices using cross-agent SND as the constraint; for each task, we perform a grid search over target SND values and report the best-performing variant.

Capability-Aware Shared Hypernetworks (CASH) [Fu et al., 2025]. Allocates behaviors at every timestep via a hypernetwork conditioned on capabilities when available, or agent identities

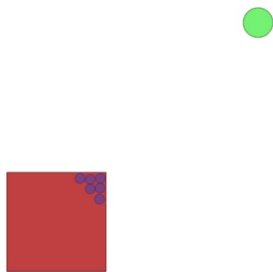
In nearly all environments, our method and the majority of baselines exhibit stable convergence toward high mean rewards, demonstrating that training is well-configured. The exception is CASH (Fig. 6a and 6b), which exhibits “shaky” performance and, in some independent runs, fails to converge to a competitive reward (Fig. 6c). We attribute this behavior to the policy brittleness inherent to its architecture. Because CASH requires re-querying the hypernetwork at every timestep to generate agent-specific weights, the resulting policy can be highly sensitive to minor fluctuations in the hypernetwork’s output. For DiCo, we evaluated several SND values and picked the one with best performance to ensure a fair comparison; the specific values used for each environment are detailed in Table 1.



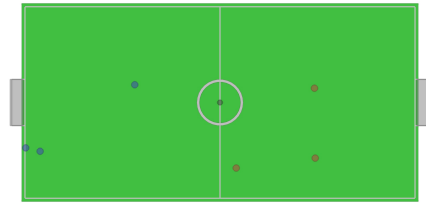
(a) Dispersion



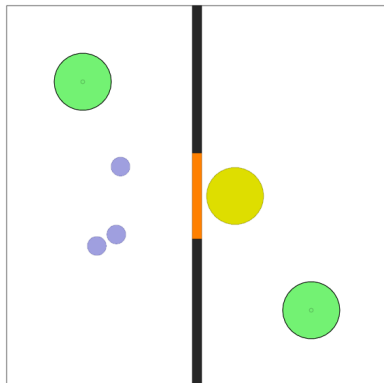
(b) Navigation



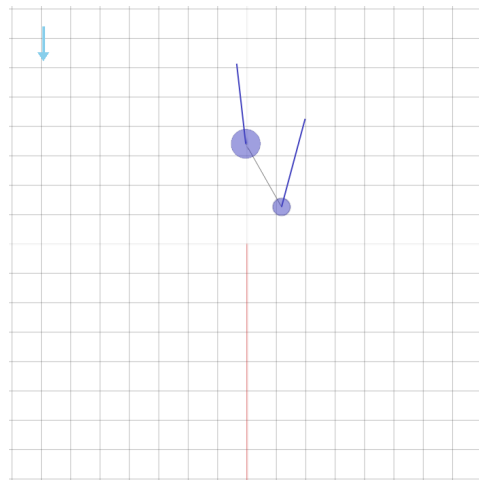
(c) Reverse Transport



(d) Football



(e) Pressure Plate



(f) Wind Flocking

Figure 5: Overview of the six tasks: (a) Dispersion, (b) Navigation, (c) Reverse Transport, (d) Football, (e) Pressure Plate, and (f) Wind Flocking.

Table 1: Hyperparameters used in the experiments.

Hyperparameter	Value / Configuration
Shared Environment & Execution Setup	
Total Training Steps	10^7
Total Training Steps for Football	150×10^6
Parallel Environments	128
Time steps for Navigation & Dispersion	200
Time steps for Reverse Transport & Football	300
Total Number of Mini-batches	8
Shared MAPPO & Optimization Parameters	
Optimizer	Adam
Adam β_1	0.9
Adam β_2	0.999
Adam ϵ	1×10^{-5}
Discount Factor (γ)	0.99
GAE Parameter (λ)	0.95
Clipping Parameter (ϵ)	0.2
Entropy Coefficient	0.01
Value Function Coefficient	0.5
Max Gradient Norm	0.5
Proposed Framework	
Homogeneous Network Size	[128, 128]
Critic Hidden Dimension	[128, 128]
Learning Rate	6×10^{-4}
Transformer Layers (Blocks)	2
Attention Heads	2
Embedding Dimension	64
MLP Hidden Dimension	256
LoRA Rank	8
DiCo Baseline Bettini et al. [2024a]	
Homogeneous Network Size	[128, 128]
Heterogeneous Network Size (Per-Agent)	[128, 128]
Learning Rate	1×10^{-4}
SND Values Tested (Grid Search)	0.1, 0.2, 0.5, 0.9, 1.0, 1.1, 1.5, 2.0
Best SND for Navigation and Dispersion	1.0
Best SND for Reverse Transport	0.1
Best SND for Football	0.2
HyperMARL Baseline Tessera et al. [2025]	
Network Size (Hypernetwork)	64
Network Size (Agents)	[64, 64]
Learning Rate	5×10^{-4}
Embedding Dimension (e_t^i)	8
CASH Baseline Fu et al. [2025]	
Policy Hidden Dimensions	[128, 128]
Critic Hidden Dimension	[128, 128]
GRU Hidden Dimension	128 (1 layer)
Learning Rate	2×10^{-3}
Hypernetwork Hidden Dimension	64
Hypernetwork Layers	4
Decoder Hidden Dimension	64
Use Two-Layer Decoder	True

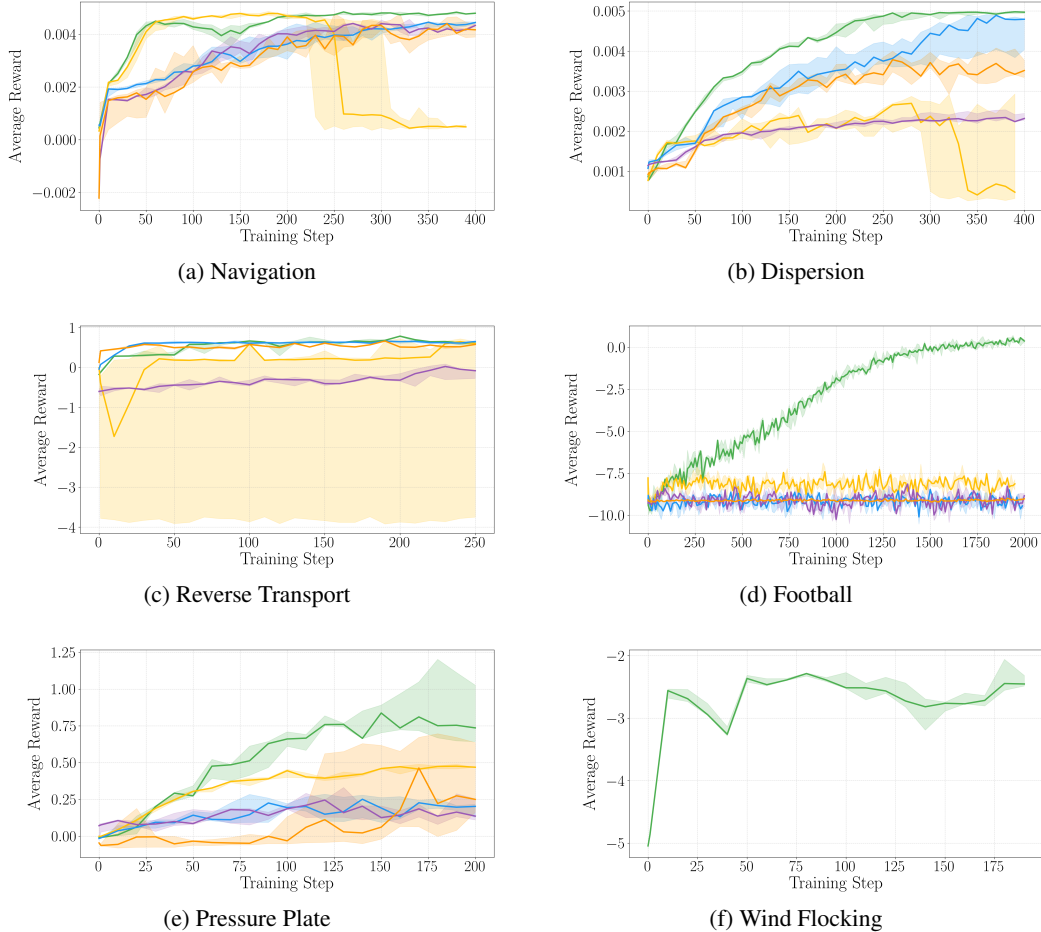


Figure 6: **Comparison of mean rewards across all evaluation tasks.** Learning curves for all the tasks. Colors denote the different methods evaluated: Ours (green), Full Parameter-Sharing (purple), CASH [Fu et al., 2025] (yellow), HyperMARL [Tessera et al., 2025] (orange), and DiCo [Bettini et al., 2024a] (blue). Performance is averaged over 5 seeds.

D.2 LoRA Rank Ablation

We conducted an ablation study on the navigation task across five independent seeds to determine the optimal rank for the Low-Rank Adaptation (LoRA) modules. Based on these results, illustrated in Fig. 7, we utilized a rank of $r = 8$ for all subsequent experiments. This configuration proved to be the “sweet spot” for our architecture, providing sufficient expressivity while maintaining the stability of the hypernetwork during training. In this sense, we recall that the dimensionality of the LoRA rank plays a critical role in the underlying optimization landscape. Restricting the hypernetwork to emit matrices $C_m \in \mathbb{R}^{r \times d}$ and $D_m \in \mathbb{R}^{d_a \times r}$, where $r \ll d$, significantly stabilizes optimization relative to generating full dense matrices.

E Broader Societal Impact

The most direct beneficiaries of event-driven behavioral adaptation are safety-critical robotic teams operating in dynamic, partially observable environments—search and rescue, post-disaster reconnaissance, environmental monitoring, and inspection of hazardous infrastructure—where agents may fail mid-mission and the optimal allocation of behaviors changes abruptly as new information arrives. The agent-removal and unseen-event experiments in Section 5 show that the team can absorb such disruptions without retraining, which is a precondition for deploying these systems outside the lab. Zero-shot generalization across team size, capability, and target diversity additionally removes the

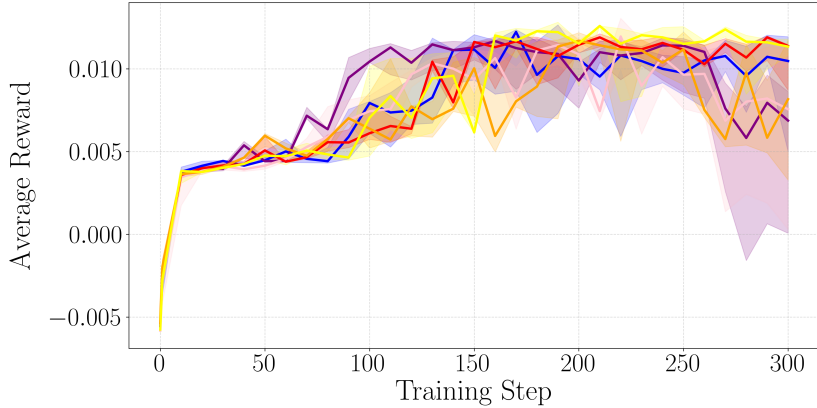


Figure 7: LoRA rank ablation in the navigation task. The plot illustrates the mean episode reward across ranks, evaluated over 5 seeds. Colors: Rank 2 (yellow), Rank 4 (orange), Rank 8 (red), Rank 16 (pink), Rank 32 (purple), and Rank 64 (blue).

need to train a separate policy for each deployment configuration, lowering the compute and energy cost of multi-robot deployment, and exposing NMD_{des} as an interpretable input scalar gives operators a post-hoc handle on team behavior without retraining. Beyond its direct technical contribution, treating behaviors as properties of the task rather than of agents carries a conceptual implication worth surfacing. Most prior MARL frameworks tie roles to agent identity, implicitly assuming that some agents are intrinsically suited to certain functions; in our framework, no agent is permanently the leader, the scout, or the helper, and any agent can instantiate any behavior the task requires at the moment it requires it. We see this as a more democratic model of cooperation, in which roles emerge from circumstance rather than from identity.

On the negative side, improvements in cooperative MARL are dual-use: the same properties that benefit search-and-rescue can in principle be applied to coordinated autonomous swarms in military or surveillance contexts. We do not believe our contribution unlocks fundamentally new capabilities along this axis but we acknowledge that more reliable team coordination is a building block that can be repurposed. A separate concern, noted as a limitation in Section 6, is that our hypernetwork is centralized and ingests observations from all agents, which raises both privacy considerations (when observations include sensor data from environments containing people) and security considerations (a single point of failure for the team’s behavioral allocation); the decentralized extension discussed in Section 6 is therefore a meaningful mitigation as well as a methodological direction.